Finite Element Analyses of the Penetration Depth of Ogive-nosed Projectiles into Conventional and Very-High Strength Concrete Targets

Girum Urgessa and Robert Sobeski
George Mason University, Fairfax, VA, USA
Email: gurgessa@gmu.edu

***Abstract*—The objective of this paper is to present the development and assessment of finite element (FE) models used for analyzing projectile penetration depth in targets made from conventional (23 MPa) to very-high strength concretes (157 MPa). Results from the FE models were compared with experimental values. The effects of varying concrete compressive strength, projectile diameter, nose shape, and striking velocity on the penetration depth of the targets were captured. Two concrete constitutive material models, the Holmquist-Johnson-Cook and the Advanced Fundamental Concrete models, were implemented in the FE analyses for determining their suitability in predicting penetration mechanics with reasonable accuracy. In most cases, the finite element results were able to predict penetration depth experimental values within a total root mean square of 10% or less considering a wide-range of projectile striking velocities. Both concrete constitutive models were shown to be suitable for penetration mechanics problems. However, based on the findings of this paper, caution should be exercised in applying the material models for targets made from harder aggregates such as quartz.**

***Index Terms*—projectile penetration, impact, very-high-strength concrete, finite element analyses, HJC, AFC**

I. Introduction

Extensive research in the last twenty years has resulted in high strength concrete that has six to eight times the strength of conventional concrete [1], [2]. Thus, the determination of projectile penetration depth using impact mechanics principles or computational methods should be reevaluated for a wide range of targets made from conventional to very-high strength concretes. There are currently three main approaches for determining the impact mechanics of concrete targets subjected to projectiles. These include empirical, analytical and numerical methods [3].

The first approach is using empirical methods that are based on simplified algebraic equations developed from data points collected through small-scale or large-scale experimental tests. However, these methods do not provide insight into material behavior during projectile penetration. A list of empirical methods used to predict projectile penetration of non-deformable and deformable missiles into concrete targets is provided in [4], [5], [6]. The second approach is using analytical methods, which are based on solving differential equations of continuum mechanics. However, these methods typically rely on simplified material properties that are necessary to arrive at closed-form solutions. The classical cavity expansion model is one example that was thoroughly reviewed [7]. The third approach is using numerical methods that are based on arriving at numerical solutions of the governing differential equations of equilibrium through finite difference or finite element methods. The objective of this paper is to present the development and assessment of finite element (FE) models used for analyzing projectile penetration depth in both conventional and very-high strength concrete targets, and to present comparison of the results of the FE models with an experimental database generated from publicly available projectile penetration tests.

II. Database of Projectile Penetration

The investigation of depth of penetration of projectiles on concrete targets using finite element analyses is typically constrained by the lack of statistically significant amount of experimental data needed for validation. In addition, most of the scarce experimental data available in the open literature lacks the appropriate associated material tests needed to characterize constitutive properties fully. In this paper, 7 projectile penetration data sets, consisting of 41 different projectile striking velocities, were identified and documented before commencing the development of the finite element models. Fig. 1 shows the extent of the experimental database.

Data sets #1 to #4 were based on experiments conducted using a 76.2 mm (3 in) diameter projectile, while the data sets #5 to #7 were based on experiments conducted using a 26.9 mm (1.1 in.) diameter projectile. For brevity, the 76.2 mm (3 in.) diameter projectiles are referred to as large projectiles and the 26.9 mm (1.1 in.) projectiles are referred to as small projectiles in this paper. All projectiles were made out of 4340 Rc45 steel and had ogive-shaped noses. The mass of the large projectiles was about 13 times the mass of the small projectiles.

Manuscript received December 26, 2018; revised June 3, 2019.

doi: 10.18178/ijscer.8.3.188-195

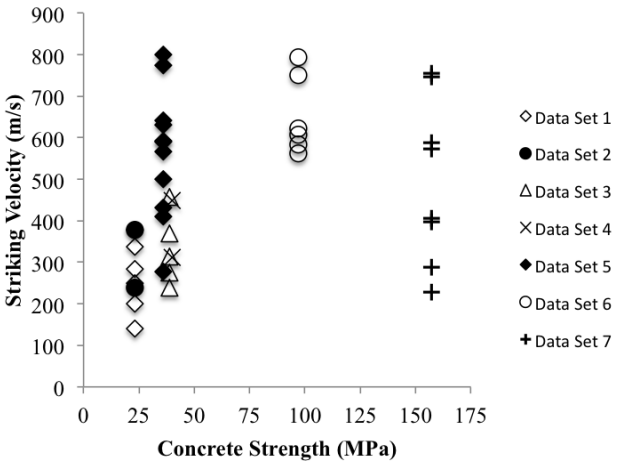

Figure 1. Experimental database of projectile penetration tests

Forrestal et al. [8] published depth of penetration data for ogive-nosed projectiles impacting 23 MPa (3.3 ksi) and 39 MPa (5.7 ksi) concrete strengths. The 23 MPa (3.3 ksi) concrete was mixed using hard aggregate while the 39 MPa (5.7 ksi) concrete was mixed using limestone aggregate. The density of the quartz mixture was 2040 kg/m^3 (0.074 lb/in^3) and the density of the limestone mixture was 2250 kg/m^3 (0.081 lb/in^3). Compressive strength tests and penetration tests were conducted between 140 and 460 days after concrete placement. The projectiles used in the tests were machined from 4340 Rc45 steel. The reported strength of 4340 Rc45 steel at high strain rates was an order of magnitude larger than the strengths of the concretes tested. The projectiles were launched using an 83 mm (3.3 inch) powder gun. Striking velocities, which did not exceed 500 m/s (1640 ft/s) because of the gun limitations, were measured using a Hall Intervalometer System. Each of the projectiles contained a void, which allowed for the insertion of a MilliPen single-channel accelerometer and data recorder. Measurements of the projectile's deceleration in the target were available. Pitch and yaw angles were determined by evaluating pictures from a high-speed digital framing camera. Pitch and yaw did not exceed 4 degrees, and are therefore are assumed normal. Tests showed that a conical entry crater about two projectile diameters deep was formed followed by a circular tunnel region slightly wider than the projectile diameter. Little to no deformation or abrasion of the projectiles occurred during the experiments and consequently they were reused as needed.

On another effort, Forrestal et al. [9] published depth of penetration data for ogive-nosed projectiles impacting 36 MPa (5.2 ksi) and 97 MPa (14.1 ksi) concrete. The density of the 36 MPa (5.2 ksi) and 97 MPa (14.1 ksi) concrete was 2370 kg/m^3 (0.086 lb/in^3) and 2340 kg/m^3 (0.085 lb/in^3) respectively. Concrete samples were taken at the time of mixing to test the unconfined compressive strength of the concrete, but these compression tests were not performed until the time of the experiment. The projectiles were machined from 4340 steel and heat-treated to a hardness of Rc45. All penetration experiments were conducted between 30 and 60 days after concrete placement. For all trials, the projectiles impacted normal to the target with the pitch and yaw measurements less than one degree. Striking velocities during these tests reached as high as 800 m/s (2600 ft/s).

O'Neil et al. [10] published depth of penetration data for ogive-nosed projectiles impacting very-high strength concrete with a compressive strength of 157 MPa (22.8 ksi). Striking velocities were measured using a streak camera. Pitch and yaw were kept under 4 degrees and were measured using flash X-rays just prior to impact. Projectiles were fitted with plastic sabots and obturators to fit a smooth bore gun. The very-high strength concrete was made by carefully selecting aggregate material to improve gradation and increase density. In the mix, reactive materials were maximized and water content was minimized. Pressure was applied prior to setting and then heat treatment was applied after setting. The result was concrete with strengths several times greater than conventional concrete. It was reported that the depth of penetration into the 157 MPa (22.8 ksi) concrete targets was about 50% of the depth of penetration into 36 MPa (5.2 ksi) concrete targets.

III. Finite Element Models

A. EPIC

Projectile penetration tests are typically expensive. With the advent of finite element analyses, multiple penetration scenarios, material flow, and stresses can be examined for a range of striking velocities as long as the models are validated by experimental data. Hence, finite element analyses of the penetration problem was performed using the 2011 Elastic Plastic Impact Computation (EPIC) code. EPIC is an explicit Lagrangian Finite Element Analysis (FEA) code developed to model short-duration high-velocity impacts [11].

To capture the complexity of the problem, the effects of varying concrete compressive strength, projectile diameter, nose shape, and striking velocity on the penetration depth of a concrete target were analyzed. Both EPIC and a post-processor called Tecplot were run on a High Performance Computing System, which is part of the United States Department of Defense Supercomputing Resource Center. EPIC was located on the Garnet machine, a Cray XE6 running a Linux operating system that can be accessed remotely through different login nodes. All finite element runs were submitted to and managed by a batch queuing system.

B. Geometric Models of the Projectiles and Targets

The 3-D geometries and finite element meshes of the projectiles and targets were created using the CUBIT Automated Geometry and Mesh Generation Toolkit [12]. All models were developed as 3-dimensional half geometries that were symmetrical about their X-Z plane and set at Y=0. The use of half-geometries resulted in computational time saving and provided improved visibility of the velocity vectors of the target without slicing the geometry through the center. Table 1 shows

the variations of projectiles used in this study. Fig. 2 and Fig. 3 detail two variations of the large projectiles (76.2 mm) that were developed to resemble the projectiles used in the experimental datasets #1 to #4. The first variation of the large projectile had a Caliber Radius Head (CRH) of 3, while the second variation of the large projectile had a CRH of 6. The CRH is a measure of nose pointiness. It is related to the radius of the ogive and the diameter of the projectile. The tail of the projectile flares out to 80.01 mm and the nose of the projectiles is flat. The flattened nose has a radius of 3.18 mm.

TABLE I. PROJECTILE CONFIGURATIONS

Type	Mass (kg)	CRH	Length (mm)	Nose Diam. (mm)	Tail Diam. (mm)	CG from tail (mm)
1	13	3	530.73	76.2	80.01	251.46
2	13	6	528.47	76.2	80.01	239.34
3	0.91	2	242.40	26.9	26.90	113.90

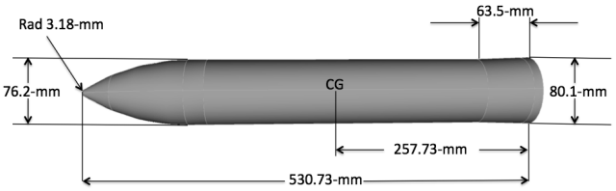

Figure 2. Large projectile (CRH = 3)

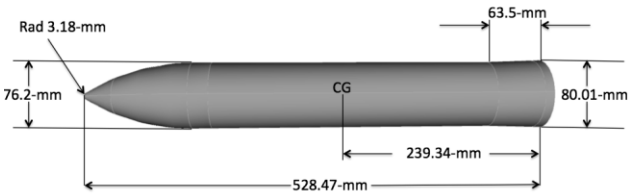

Figure 3. Large projectile (CRH = 6)

Fig. 4 details the small (26.9 mm) projectile that was developed to resemble the projectiles used in the experimental data sets #5 to #7. The small projectile had a CRH of 2. The type of projectile used in these experiments was hollow containing approximately 166 mm by 10 mm void along its longitudinal axes. The placement and exact size of the void were adjusted during geometry development to fit the mass and center of gravity of the projectiles.

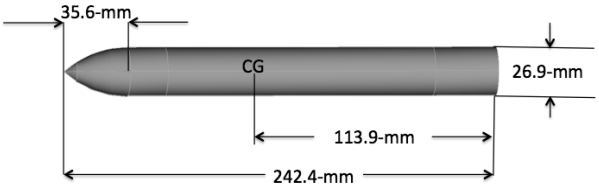

Figure 4. Small projectile (CRH = 2)

An automatic meshing function could not determine a meshing solution on its own for this particular geometry of the projectiles. Therefore, to mesh the nose, each curve in the sub-volume was first assigned an interval ensuring that the intervals matched along opposite edges of the geometry. The surfaces of the wedge-shaped ends were then meshed using a pave meshing scheme. The pave scheme automatically meshes an arbitrary three-dimensional surface with quadrilateral elements [13], [14]. The paver allows for easy transitions between dissimilar sizes of elements and element size variations, such as the curved pointy nose of the projectile.

The generated mesh is well formed with nearly square elements that are perpendicular to the boundaries. The three remaining surfaces on the volume were meshed using the map mesh scheme. The map mesh scheme meshes a surface (or volume) with quadrilaterals (or hexahedra) where each interior node on a surface (or volume) is connected to 4 (or 6) other nodes. Finally, the volume was meshed using the sweep-meshing scheme in a direction from the curved nose surface to the opposite planar end of the sub-volume. The sweep scheme can mesh a volume by translating or rotating a topologically similar surface along a single axis from a source surface to a target surface [15], [16]. The larger (76.2 mm) projectile was created in a similar fashion as the smaller projectile, but required extra sub-volumes to account for the blunt nose of the projectile.

Care had been taken to start the meshing process at the nose of the projectile and then proceeding towards the tail of the projectile in order to get the volume to mesh properly. For all the seven data sets investigated, the concrete targets were cast inside galvanized corrugated steel culverts. As such, each target had a cylindrical geometry, but the height and radius of the cylinder varied. Fig. 5 shows a typical half-cylindrical target geometry with the projectile.

Figure 5. Target-projectile pair

The culvert diameters ranged from 0.76 m to 1.83 m in the experimental tests. In all cases, the target-diameter to projectile-diameter ratio was at least 24. This ratio ensured that no large cracks would reach the outer edge

of the concrete thereby preventing the possibility og getting misleading depth of penetration values. In the finite element models, the projectile-diameter ratio was assumed to be sufficiently large such that the culvert's presence would not be noticed. This assumption was verified by running two initial finite element models with and without the culvert in place for data set #5 at 600 m/s. The results of these two finite element initial runs showed that the presence of the culvert had no effect on the depth of penetration. Furthermore, a similar analysis on the effects of using soakers on the outer surface of the target was investigated. It was verified that the target's surface boundaries were too far from the penetration event to play any significant role in the penetration depth.

The target lengths for the experimental data sets varied from 0.76 m to 1.83 m. In all cases, the length of the target was at least twice the depth of penetration. The concrete strengths varied from 23 MPa (3.3 ksi) to 157 MPa (22.8 ksi) as shown in Fig. 1. The 3-D half-geometries of the projectiles and targets were created using hexahedron elements, but were later converted to tetrahedrons using EPIC's pre-processor. EPIC converts each hexahedron element into 24 tetrahedrons. This two-step meshing process ensured that the tetrahedral elements were arranged in a symmetric manner, thereby minimizing the potential for unwanted tetrahedral mesh locking.

C. Material Models

During short-duration high-velocity impacts, it is very difficult to measure stresses, strains, pressures, and temperatures with a degree of certainty. Consequently, a constitutive model of material behavior that can reasonably capture the physical phenomena is needed. One of the reason for choosing EPIC in this study is because of its library of concrete material models that are readily available for use in short-duration dynamic events. The two concrete constitutive models included in this study are the Holmquist-Johnson-Cook (HJC*) model [17] and the Advanced Fundamental Concrete (AFC) model [18]. The material model parameters are derived from wave propagation experiments such as split-Hopkinson bar, plate impact tests, expanding ring tests, and coplanar bar impacts.

The HJC* concrete model is a computational constitutive model for concrete that includes the effects of material damage, high strain rate, and permanent crushing. The model relates the normalized equivalent stress in concrete to the normalized pressure by the relationship shown in (1) where σ^* is the equivalent stress normalized by the unconfined compressive strength, D is the damage factor, P* is the normalized pressure, ε^* is the dimensionless strain rate, A is the normalized cohesive strength, B is the normalized pressure hardening coefficient, N is the pressure hardening exponent, and C is the strain rate coefficient. If D = 0, the concrete is undamaged, and if D = 1, the concrete is fractured.

$$\sigma^* = [A(1-D) + BP^{*N}][1 + C\ln\dot{\varepsilon}] \quad (1)$$

The model accumulates damage from equivalent plastic strain and plastic volumetric strain. The asterisks represent normalization by dividing the value by the unconfined compressive strength of the concrete. Three pressure-volume response regions are considered. The first region is the linear elastic region, which occurs when the pressure is less than the crushing pressure. The second region is the transition region, which occurs between the crushing pressure and the locking pressure. The third region is the comminuted region, which occurs above the locking pressure and it is where the concrete is compressed into a fully dense material. Porous materials like concrete compact irreversibly under compression, crack and separate in tension, and yield under shear. As pressure increases, however, the shear strength increases as well. Pressure constants are obtained from shock Hugoniot data. The HJC* model requires inputs for up to 30 model parameters, which can be grouped into six categories. These are mass/thermal properties, strength properties, pressure properties, artificial viscosity, facture properties, and total failure strain. Understandably, it was extremely difficult to characterize all 30-model parameters accurately. With knowledge of a few key parameters, however, reasonable results can be achieved by approximating the less sensitive parameters. Thacker [19] conducted a probabilistic sensitivity analysis of the HJC* concrete model parameters and developed an importance ranking of the model parameters in conventional strength concrete. It was shown that the unconfined compressive strength had the most influence on the computed penetration depth. Therefore, in our research, the unconfined compressive strength is used as main comparative model parameter across the experimental data sets.

On the contrary, the AFC model simulates irreversible hydrostatic crushing, material yielding, plastic flow, and material damage. The AFC model has a nonlinear, pressure-volume relationship, a linear shear relationship, strain-rate hardening effects for the failure surface, and it separates the hydrostatic response from the deviatoric response. The compressive hydrostatic behavior in the AFC model is the same model as used in the HJC* model. The shear behavior model, however, varies based upon the sign of the first invariant (tension vs. compression) and by a factor that is a function of the third invariant of the deviatoric stress tensor. This allows the model to differentiate between the extension and compression failure surfaces due to the inclusion of the third invariant.

For each experimental data set, two finite element models were run with the HJC* and AFC constitutive material models for comparison purposes.

IV. Results and Discussions

The experimental database presented in Fig. 1 has a total of 41 data points spanning across 7 grouped data sets. Multiple finite element models were run because two constitutive material models were examined for each case. Fig. 6 presents a typical global output. As a projectile penetrates into a concrete target at high velocity, the target mesh becomes severely distorted along the

projectile-target interface. Severe grid distortions are a problem for Lagrangian codes because the time step is often coupled to the size of the smallest element in the mesh. Further, depending upon mesh geometry, severe distortions can sometimes cause local stiffening and locking of the mesh. The approach taken in this study to mitigate this issue is to convert severely distorted elements into meshless particles.

The conversion option works well on concrete penetration problems because physically, the concrete along the projectile-target boundary exceeds its failure point during this event. The comminuted concrete has no tensile stresses, but continues to have mass, volume, velocity and compressive strength similar to meshless particles. As the projectile moves forward, it continues to exert force on the meshless particles forcing them to interact with the intact concrete elements or to move up and out towards the entry point of the target. The predicted movement of comminuted concrete out of the projectile tunnel is consistent with observed material behavior during penetration experiments [20], [21], [22].

It is worth noting that the alternative approach for handling extremely distorted elements is by using an erosion procedure. In erosion, the highly distorted elements are simply removed from the model leaving a void in the place of the distorted elements based on a pre-defined limit such as element failure strain. Details of erosion algorithms are extensively covered in literature [3], [23], [24], [25]. However, erosion typically results in over-prediction of penetration depths because the presence of voids allows the projectile to move forward and occupy the empty space without incurring the resistive forces afforded by meshless particles. Hence, the erosion procedure was not implemented in this study.

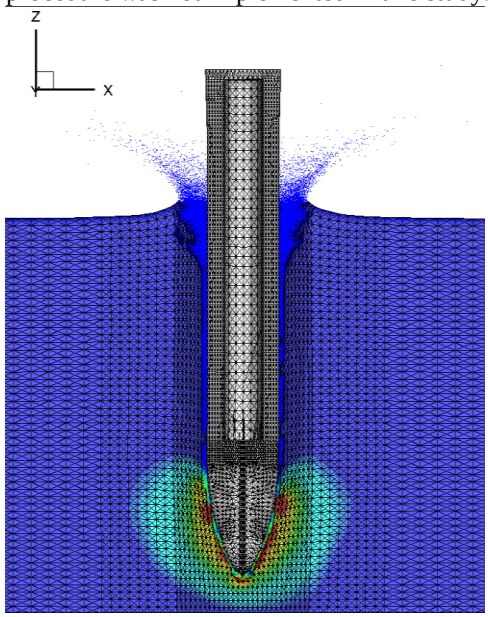

Figure 6. Projectile penetration and meshless particles

Overall, the finite element models predicted the depth of penetration very well when compared to the experimental data sets #3, #4, #5, #6, and #7. However, the finite element models did not necessarily perform well with the results of the experimental data sets #1 and #2, and possible reasons are discussed in detail later at the end of this section.

Fig. 7 shows finite element results for data set #3 where the large projectile with 3 CRH penetrated into a 39 MPa (5.7 ksi) concrete target. Here, the HJC* material model predicts the depth of penetration with a total root-mean-square (RMS) error of 11% across the overall range of striking velocities. However, it performed exceptionally well for striking velocities below 375 m/s. If the experimental data at 450 m/s was not included in the RMS calculation, the RMS error for the HJC* material model would be 1.8%. The AFC material model had a total RMS error of 12.6%. While it fits the experimental data at 450 m/s better than the HJC* model, it predicted higher depth of penetration values at lower striking velocities.

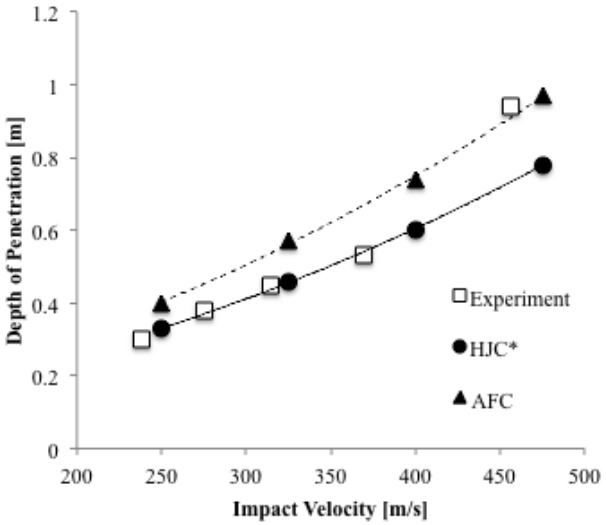

Figure 7. Penetration depth results for data set #3

Fig. 8 shows finite element results for data set #4 where the large projectile with 6 CRH penetrated into a 39 MPa (5.7 ksi) concrete target. Here, the AFC material model predicted the depth of penetration better than the HJC material model when compared to the experimental data for the entire range of striking velocities. The AFC predictions had a total RMS error of 3.2% while HJC* predictions had a total RMS error of 12.2%.

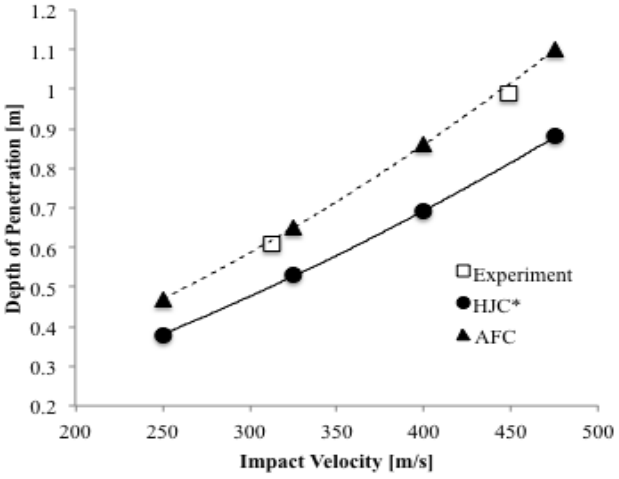

Figure 8. Penetration depth results for data set #4

Fig. 9 shows finite element results for data set #5 where the small projectile with 2 CRH penetrated into a 36 MPa (5.2 ksi) concrete target. Here, the HJC* material model consistently provided lower penetration depth values when compared to the experimental tests with a total RMS error of 6%. The AFC material model performed well in the 200-600 m/s striking velocity range with a total RMS error of 9.6%.

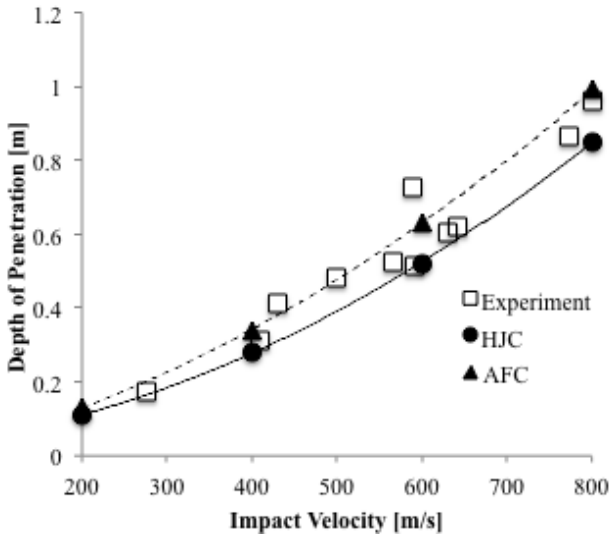

Figure 9. Penetration depth results for data set #5

Fig. 10 shows finite element results for data set #6 where the small projectile with 2 CRH penetrated into a 97 MPa (14.1 ksi) concrete target. Results from both the HJC* and AFC models agree very well when compared to experimental values, particularly for striking velocities of less than 700 m/s. The HJC* material model resulted in a total RMS error of 7.7% and the AFC material model resulted in a total RMS error of 4.8%.

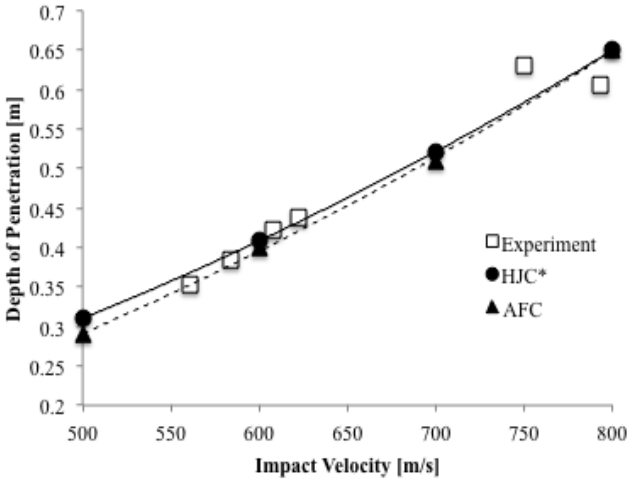

Figure 10. Penetration depth results for data set #6

Fig. 11 shows finite element results for data set #7 where the small projectile with 2 CRH penetrated into a 157 MPa (22.8 ksi) very-high strength concrete target. Results from both the HJC* and AFC material models agree very well when compared to experimental values. The HJC* material model resulted in a total RMS error of 4.1%, while the AFC material model resulted in a total RMS error of 3.5%.

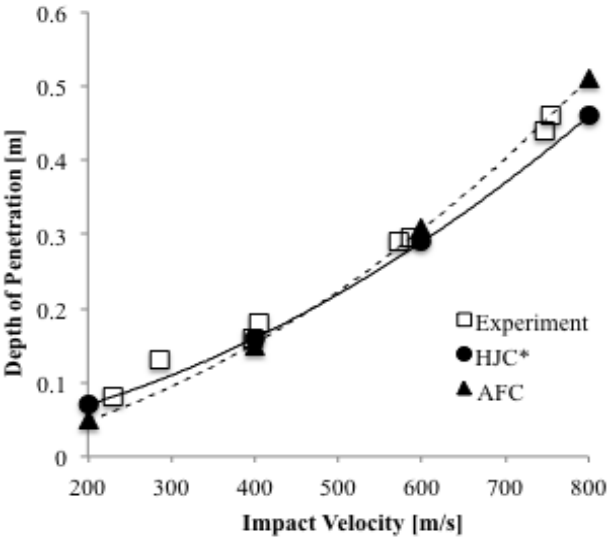

Figure 11. Penetration depth results for data set #7

Data sets #1 and #2 contained penetration depth information into 23 MPa (3.3 ksi) concrete targets made from quartz aggregate. An adequate material model was not available to characterize this type of aggregate. As such, limestone aggregate models with a compressive strength of 23 MPa were used in the finite element analyses.

Fig. 12 and Fig. 13 show the results for data set #1 and #2 respectively. It was clear that the HJC* material models predicted the penetration behavior very well whereas the AFC material model results did not adequately reflect the experimental data, particularly at higher striking velocities.

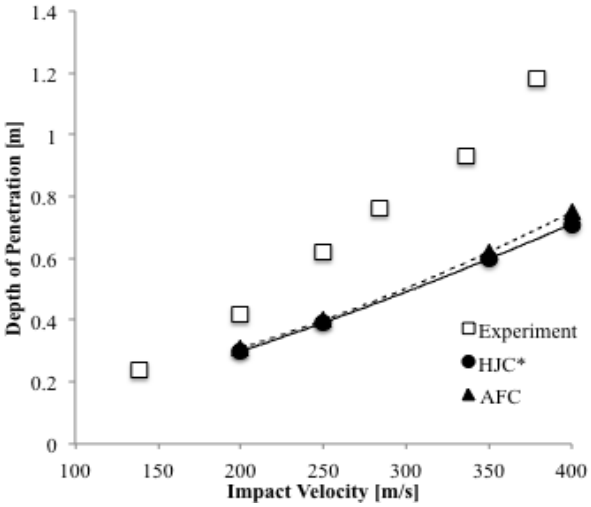

Figure 12. Penetration depth results for data set #1

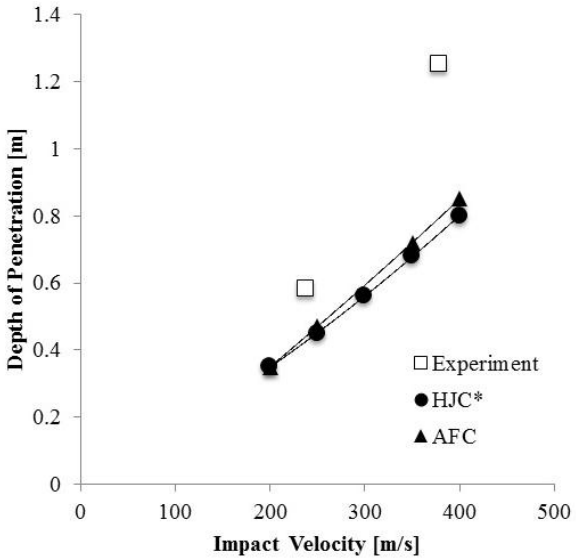

Figure 13. Penetration depth results for data set #2

V. Conclusions

The development of finite element (FE) models used for analyzing projectile penetration depth in targets made from conventional (23 MPa) to very-high strength concretes (157 MPa) was presented. Seven projectile penetration data sets, consisting of 41 different projectile striking velocities, were identified and documented for comparing results from the finite element analyses.

The effects of varying concrete compressive strength, projectile diameter, nose shape, and striking velocity on the penetration depth of the targets were studied. In addition, two concrete constitutive models, the Holmquist Johnson Cook and the Advanced Fundamental Concrete models, were implemented in the FE analyses for determining their suitability in predicting penetration mechanics within reasonable accuracy.

For penetration problems in the velocity regime of this study (200-800-m/s), the steel projectiles remained intact, and little to no projectile material underwent distortions great enough to require conversion. This rigid-projectile model behavior is supported by the state of post-impact projectiles where little to no deformations were observed.

In most cases, the finite element results were able to predict penetration depth experimental values within a total root mean square of 10% or less considering a wide-range of projectile striking velocities.

Both concrete constitutive models were shown to be suitable for penetration mechanics problems. However, based on the findings of this paper, caution should be exercised in applying the material models for targets made from harder aggregates.

Acknowledgment

The authors wish to thank Dr. James Cargile of the United States Army Corps of Engineers (USACE) Engineer Research and Development Center (ERDC) for his valuable expertise, help, and insights on penetration mechanics of concrete targets.

References

[1] J. D. Cargile, E. F. O'Neil and B. D. Neeley, "Very-High-Strength Concretes for Use in Blast- and Penetration-Resistant Structures," The AMPTIAC Quarterly, vol. 6, no. 4, pp. 61-67, 2011.
[2] FHWA. *Ultra-High Performance Concrete*. TECHNOTE. McLean, VA, Federal Highway Administration, 2011.
[3] J. A. Zukas, *Introduction to Hydrocodes*, Studies in Applied Mechanics, 49, Elsevier, 2004.
[4] M. Y. H. Bangash, *Shock, Impact and Explosion: Structural Analysis and Design*, Springer, 2009.
[5] I. A. Rahman, A. M. A. Zaidi and Q. B. Latif, "Review on Empirical Studies of Local Impact Effects of Hard Missile on Concrete Structures," *International Journal of Sustainable Construction Engineering and Technology*, pp. 73-97, 2010.
[6] P. C. Stivaros and A. J. Philippacopoulos, "Structural Evaluation of Reinforced Concrete Bunkers in High Speed Balancing Facilities," ACI Special Publication SP281-05, pp. 1-18, 2011.
[7] R. Sobeski and G. Urgessa, "Review of Quasi-analytical and Cavity Expansion Methods for Projectile Penetration of Concrete Targets," *International Journal of Protective Structures*, vol. 6, no. 1, pp. 43-64, 2015.
[8] M. J. Forrestal, D. J. Frew, J. P. Hickerson and T. A. Rohwer, "Penetration of Concrete Targets with Deceleration-time Measurements," *International Journal of Impact Engineering*, vol. 28, pp. 479-497, 2003.
[9] M. J. Forrestal, B. S. Altman, J. D. Cargile and S. J. Hanchak, "An Empirical Equation for Penetration Depth of Ogive-nose Projectiles into Concrete Targets," *International Journal of Impact Engineering*, vol. 15, no. 4, pp. 395-405, 1994.
[10] E. F. O'Neil, B. D. Neeley and J. D. Cargile, *Tensile Properties of Very-High Strength Concrete for Penetration Resistant Structures*, U.S. Army Engineer Research and Development Center, 2000, Vicksburg, MS.
[11] G. R. Johnson, *EPIC-3, A Computer Program for Elastic-Plastic Impact Calculations in 3 Dimensions*, BL 343, AD-058786, Defense Systems Div., 1977.
[12] Sandia National Laboratory, *CUBIT 14.1 User Documentation*, 2014.
[13] T. D. Blacker and M. B. Stephenson, "Paving: A New Approach to Automated Quadrilateral Mesh Generation," *International Journal of Numerical Methods*, vol. 32, pp. 811–847, 1991.
[14] G. Urgessa, S. Horton, M. M. R. Taha and A. K. Maji, "Significance of Stress-block Parameters on the Moment Capacity of Sections Under-reinforced with FRP," *ACI SP 230-87*, pp. 1531-1550, 2005.
[15] W. Ali and G. Urgessa, "Numerical Prediction Model for Temperature Distributions in Concrete at Early Ages," *American Journal of Engineering and Applied Science*, vol. 5, no. 4, pp. 282-290, 2012.
[16] G. Urgessa, "Finite Element Analysis of Composite Hardened Walls Subjected to Blast Loads," *American Journal of Engineering and Applied Science*, vol. 2, no. 4, pp. 804-811, 2009.
[17] T. J. Holmquist, G. R. Johnson and W. H. Cook, "A Computational Constitutive Model for Concrete Subjected to Large Strains, High Strain Rates, and High Pressures," *Fourteenth International Symposium on Ballistics*, 1993.
[18] M. D. Adley, A. O. Frank, K. T. Danielson, S. A. Akers and J. O'Daniel, *The Advanced Fundamental Concrete (AFC) Model (TR10-51)*, 2010.
[19] B. H. Thacker, *Probabilistic Sensitivity Analysis of the Holmquist-Johnson-Cook Material Model for Concrete (SWRI 18-02947)*, 2000.
[20] C. Y. Tham, "Reinforced Concrete Perforation and Penetration Simulation using AUTODYN-3D," *Finite Elements in Analysis and Design*, vol. 41, pp. 1401-1410.
[21] R. Sobeski and G. Urgessa, "Concrete Material Flow during Projectile Penetration," *Proceedings of the 2014 Structures Congress, American Society of Civil Engineers*, pp. 2048-2059, 2014.
[22] D. J. Frew, S. J. Hanchak, M. L. Green and M. J. Forrestal, "Penetration of Concrete Targets with Ogive-Nose Steel Rods," *International Journal of Impact Engineering*, vol. 21, no. 6, pp. 489-497, 2006.

[23] T. Belytschko and J. I. Lin, "A Three-dimensional Impact Penetration Algorithm with Erosion," International Journal of Impact Engineering, vol. 5, no. 1-4, pp. 111-127, 1987.
[24] M. Casey and G. Urgessa, *Rebar Cage Construction and Safety: Best Practice*, American Society of Civil Engineers, 2012.
[25] F. B. Mendonca, G. Urgessa, and J. A. Rocco. "Blast Response of 60 MPa Reinforced Concrete Slabs Subjected to Non-Confined Plastic Explosive," Structures Congress, 15-26, 2017.

Girum Urgessa received a B.S. in Civil Engineering from the Addis Ababa University in 2000, and a M.S. and a Ph.D. in Civil Engineering from the University of New Mexico in 2002 and 2006 respectively.

He is currently an Associate Professor of Civil Engineering and an Affiliate Faculty of the C4I & Cyber Center at George Mason University. Prior to joining George Mason University in 2007, he was a research engineer in the Applied Science Division of Weidlinger Associates, and a structural engineer at Dekker/Perich/Sabatini both in Albuquerque, NM.

Dr. Urgessa is currently a member of the American Society of Civil Engineers SEI technical committee on dynamic effects, sub-committee on retrofit of structures under dynamic loads. He was a voting member of the American Concrete Institute technical committee on blast and impact load effects (ACI 370) and the Transportation Research Board technical committee on field testing and non-destructive evaluation of transportation structures (AFF 40). He is a licensed professional engineer in the State of Maryland in the United States.

Robert Sobeski received a B.S. in Engineering Physics from the United States Military Academy at West Point in 1992, a M.S. in Engineering Management from the University of Missouri-Rolla in 1996, a M.S. in Nuclear Engineering from the Massachusetts Institute of Technology in 2001, and a Ph.D. in Civil and Infrastructure Engineering from George Mason University in 2014.

He served as an instructor at the United States Military Academy from 2001 to 2003 and then as an Assistant Professor from 2003 to 2004. From 2004 to 2009, he worked as program manager for the Defense Threat Reduction Agency in the Research and Development Enterprise. Prior to attending George Mason University, he was assigned as the Deputy Division Chief of the Stockpile Services Division of the National Nuclear Security Administration.